On the Epochal Strengthening in the Relationship between Rainfall of East Africa and IOD

DESMOND MANATSA

Department of Geography, Bindura University of Science Education, Bindura, Zimbabwe, and Department of Ocean Technology, Policy, and Environment, University of Tokyo, Tokyo, Japan, and International Centre for Theoretical Physics, Trieste, Italy, and Research Institute for Global Change, JAMSTEC, Yokohama, Japan

SWADHIN K. BEHERA

Department of Ocean Technology, Policy, and Environment, University of Tokyo, Tokyo, and Research Institute for Global Change, JAMSTEC, Yokohama, Japan

(Manuscript received 5 August 2012, in final form 31 December 2012)

ABSTRACT

Variability of the equatorial East Africa ''short rains'' (EASR) has intensified significantly since the turn of the twentieth century. This increase toward more extreme rainfall events has not been gradual but is strongly characterized by epochs. The rain gauge–based Global Precipitation Climatology Centre (GPCC) monthly precipitation dataset for the period 1901–2009 is used to demonstrate that the epochal changes were dictated by shifts in the Indian Ocean dipole (IOD) mode. These shifts occurred during 1961 and 1997. In the pre-1961 period, there was virtually no significant linear link between the IOD and the EASR. But a relatively strong coupling between the two occurred abruptly in 1961 and was generally maintained at that level until 1997, when another sudden shift to even a greater level occurred. The first principal component (PC1) extracted from the EASR spatial domain initially merely explained about 50% of the rainfall variability before 1961, and then catapulted to about 73% for the period from 1961 to 1997, before eventually shifting to exceed 82% after 1997. The PC1 for each successive epoch also displayed loadings with notably improved spatial coherence. This systematic pattern of increase was accompanied by both a sharp increase in the frequency of rainfall extremes and spatial coherence of the rainfall events over the region. Therefore, it is most likely that the 1961 and 1997 IOD shifts are responsible for the epochal modulation of the EASR in both the spatial and temporal domain.

1. Introduction

Changes in rainfall patterns have severe consequences for the already hard-pressed and impoverished national economies of Africa, adding an immense environmental stress to a region with a reduced capacity to adapt to the mounting adverse effects of global warming. East Africa, in particular, has in recent years experienced increased frequencies in both extreme flooding and severe droughts. In this region that is characterized by sparse water resources, this change has serious impacts on millions of people and is posing unparalleled threat to the community and its environment (Shongwe et al. 2011). Perhaps that is why East Africa's climate appears to be the most extensively studied part of the African continent, even though many issues related to the rainfall's modulation remain largely unresolved.

The region's seasonal rainfall regime is composed of two distinct seasons locally known as the ''long rains,'' occurring from March to May (MAM), and the ''short rains,'' taking place from October to December (OND). While the long rains are associated with the relatively slow northward movement of the ITCZ, the short rains are related to a more rapid southward migration of this phenomenon (Black et al. 2003). Thus, comparatively, precipitation events during the long rains season tend to be less variable, heavier, and longer in duration, with less interannual variability, and are more likely to be associated with local factors (Mutai and Ward 2000). In

Corresponding author address: Desmond Manatsa, Department of Geography, Bindura University of Science Education, Private Bag 1020, Bindura, Zimbabwe.
E-mail: dmanatsa@gmail.com

DOI: 10.1175/JCLI-D-12-00568.1

contrast, precipitation events during the short rains are less intense with shorter duration and stronger intraseasonal and interannual variability that is more coherent in space and time (Clark et al. 2003). This mirrors more of typical impacts of large-scale phenomena such as ENSO and/or the Indian Ocean dipole (IOD) during the short rains, hence our interest on this season.

Efforts have been made in explaining the rainfall variability through two of the most important tropical climate drivers, namely ENSO (Mutai et al. 1998; Reason et al. 2000; Clark et al. 2003) and the IOD (Goddard and Graham 1999; Black et al. 2003; Clark et al. 2003; Behera et al. 2005). But the increased coupling between the tropical Pacific and Indian Oceans during the ENSO cycle since the mid-1970s resulted in frequent co-occurring IOD and ENSO events (Annamalai et al. 2005). Thus, the resulting indirect effects from the Pacific via the Indian Ocean could thus have resulted in the statistical relationship between East African rainfall and ENSO described in earlier studies (e.g., Janowiak 1988) and the coincidental physical explanations offered by other more recent authors (e.g., Mutai et al. 1998; Kijazi and Reason 2009). In any case, it has now become more apparent that the relationship between the rainfall of East Africa and ENSO is actually more the result of an indirect forcing by ENSO on the Indian Ocean. Climate model simulations (e.g., Goddard and Graham 1999; Latif et al. 1999) and observation studies (e.g., Black et al. 2003; Clark et al. 2003; Behera et al. 2005) demonstrate plausible evidence of the essential role of the tropical Indian Ocean in modulating rainfall variability.

The recent rainfall characteristics of East Africa are unprecedented in duration, spatial character, intensity, and seasonal expression. Hence disasters from droughts and floods have increased in the recent decades (e.g., Shongwe et al. 2011). Understanding the causes becomes essential. In fact, SST patterns linked to the IOD and the associated changes in the basinwide atmospheric circulation are implicated in the rainfall extremes of the recent two decades over East Africa, manifesting as disastrous floods in 1997 (Latif et al. 1999; Webster et al. 1999) and the devastating drought of 2005 (Hastenrath 2007). However, most of these studies have been limited to the decades after the 1950s except for a few (e.g., Hong et al. 2008; Abram et al. 2008; Nakamura et al. 2009, 2011). In these investigations, it is quite evident that stationarity in the relationship with the associated climate drivers has been largely assumed. This assumption may prove to be costly as far as projecting the future climate of the region is concerned, as shifts have frequently punctuated regional global climates before and may still dominate the region in the future. In this regard it becomes logical that the long-term temporal impact of the IOD and East African rainfall is established and documented in view of the recently established shifts in the IOD (Nakamura et al. 2009; Manatsa et al. 2012). This may add considerable insight into the usability of the IOD as a predictor and in the climate change modeling of the related rainfall mechanisms.

The present study focuses on the OND season, not only because it coincides with the peak period of IOD activity but also, importantly, because it has greater impact on society. The East Africa short rains (EASR) season comes after the driest period of the year (stretching from June to September), is less in amount (accounting for only 30%–40% of the annual total; Vuille et al. 2005), and is less dependable due to its greater variability. In addition, it is characterized by stronger spatial coherence of rainfall anomalies across a large part of the region (e.g., Clark et al. 2003). Hence, improved understanding of its decadal to multidecadal variability and its possible triggers may enhance the long-term forecasting of this season. However, the overarching goal of the present study is to demonstrate that it is the epochal changes related more to the IOD itself (changes that are not directly related to global warming) that influenced the observed alterations in the rainfall pattern to become more extreme.

2. Data and methods of investigation

a. Data

The equatorial East Africa short rains index for the OND rainfall is based on a large-scale standardized area-average rainfall index for the region of East Africa depicted in Fig. 1. The rational for selecting this region is found in Manatsa et al. (2012). The precipitation data are from version 5 of the Global Precipitation Climatology Centre (GPCC) dataset and are for the period 1901 to 2009 with a spatial resolution of 0.5°. More details on the data and their usage in research can be found on the GPCC home page (http://gpcc.dwd.de/). To verify the representativeness of this derived time series we compared it to a Kenya World Meteorological Organization (WMO) station (63619) called Moyale with continuous rainfall data from 1915 to 2011. No significant differences were noted between the two, suggesting that the known shifts in rain gauge density that characterized the region during the period of study did not significantly affect the aerially averaged rainfall time series. To ascertain the normality of the EASR index, the following three normality tests were used: the Shapiro–Wilk test, the Anderson–Darling test, and the d'Agostino test. These tests are considered some of the most powerful statistics for detecting most departures from normality in time series.

The atmospheric reanalysis data by the U.S. National Centers for Environmental Prediction (NCEP) and

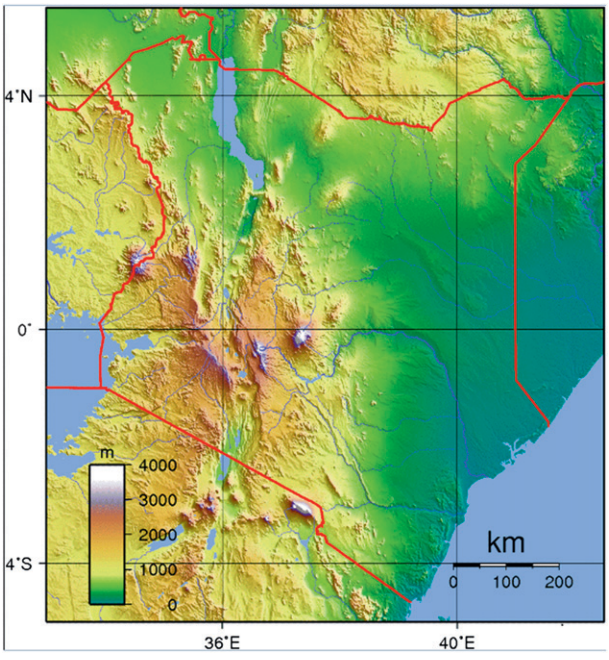

FIG. 1. Relief map for the region of equatorial East Africa from where rainfall data for EASR are extracted (Source: http://mapsof.net/map/kenya-topography).

National Center for Atmospheric Research (NCAR) (Kalnay et al. 1996) for the period 1948–2009 are also used. Although we use these synthetic data to interpret observations, the assimilated data are far from homogeneous. Caution has to be taken as they improve over time in both quality and quantity, especially after the 1970s when the satellite era begins. From this reanalysis data, we use the wind data to show large-scale tropical circulation anomalies associated with interannual rainfall variability over East Africa and outgoing longwave radiation (OLR) data to approximate convection. For spatial analysis of the sea surface temperature (SST) we used version 1 of the Met Office Hadley Centre's Sea Ice and Sea Surface Temperature dataset (HadISST1). Details of this dataset can be found online (http://apdrc.soest.hawaii.edu/datadoc/hadisst1.php). The Global Precipitation Climatology Project (GPCP) monthly precipitation dataset (v2.2; http://www.esrl.noaa.gov/psd/data/gridded/data.gpcp.html) from 1979 to the present, which combines observations and satellite precipitation data into 2.5° × 2.5° global grids, was used for precipitation analysis over the ocean. The Indian Ocean dipole index was constructed from the SST time series of the east–west SST gradient from averages over the eastern (0°–10°S, 90°–100°E) and the western (10°N–10°S, 50°–70°E) SST time series that are not normalized. The index is derived by simply calculating the SST cumulative gradient for the individual months of the OND season. The SST data are for the period 1901 to 2009 from the HadSST1 dataset extracted from the Climate Explorer website.

b. Methodology

Principal component analysis (PCA), also known as empirical orthogonal function (EOF) analysis, is a widely used technique in climate research. One of the major strengths inherent in the PC analysis is that it allows fields of highly correlated data to be represented adequately by a small number of orthogonal functions and corresponding orthogonal time coefficients without a prescribed or predetermined form. The mathematical details of this technique and how it is used are described in Jolliffe (1986). In our case we extracted for analysis only the dominant PC as it was able to reproduce, with time, most of the important variation in original rainfall data. In this way the first PC (PC1) provided an alternative and much simpler description of the data than the original rainfall field. The PC1 was then used to describe the degree of spatial coherence of the rainfall variation for each epoch demarcated by preexisting shifts so as to assist in interpreting the possible causes of the discontinuities in the spatial variability context.

Shifts were detected using the cumulative sum technique and the shift detection technique by Rodionov (2004). The former represents the running total of the deviations of the first observations from a mean based on the same interval (Ibanez et al. 1993). These are plotted over time (years) to allow one to determine the year when an abrupt change occurred. However, despite its simplicity in implementing, this approach is considered robust in detecting changepoints (e.g., Breaker 2007). The latter method provides a probability level for the identified year of regime shift in the mean and/or variance, based on the Student's t test and F test. This technique involves sequential data processing in which the testing is done in sequence. The current work uses a large cutoff length (31 yr) and a probability level of to 0.01 to confirm significance. This technique has been widely used in physical (Figura et al. 2011), biological (Overland et al. 2008), and economic contexts (Dionne et al. 2009). The software for the detection of a regime shift is available online (http://www.beringclimate.noaa.gov/regimes).

The standardized precipitation index (SPI) method is used to characterize the rainfall of East Africa. The main advantage is that this technique is able to return fundamental parameters of the occurrence of different drought/wet types in terms of severity, magnitude, and frequency. Technically, the SPI is the number of standard deviations by which the observed value deviates from the long-term mean for a normally distributed

TABLE 1. Results of normality test using various methods from Tanagra Data Mining software version 1.4.42.

Attribute	μ; sigma	Shapiro–Wilk (p value)	Anderson–Darling (p value)	d'Agostino (p value)
EASR	0.0132; 1.0092	0.8679 (0.0000)	2.1925 (0.0000)	59.0763 ($p < 0.01$)

random variable. Details about the SPI computation can be found in several papers including McKee et al. (1993) and Vicente-Serrano et al. (2004). However, the most important aspect in its calculation is that since precipitation does not show a normal distribution, data are transformed to follow a normal distribution using an appropriate transforming method. In our case no prior transformation of the rainfall data was needed since the test for normality using various methods, whose results are depicted in Table 1, yielded rainfall data that were significantly normally distributed. This means that for our OND SPIs, we basically standardized the OND anomalies for the whole period. We also refer to the resulting times series simply as the equatorial East Africa short rains index.

In Table 2 we present the SPI values, their frequency probabilities, and nominal class descriptions. We adopted the Agnew (1999) SPI nominal classification that uses the 5%, 10%, and 20% occurrence probabilities but modified it as it classifies some historical regional rainfall seasons as normal that in fact have traditionally been documented as droughts/wet seasons in East Africa. Thus the 33.3% (tercile) occurrence probability is considered, which is normally employed within the African region to define drought/wet season thresholds. In this way another class of mild drought/slightly wet is added to the original Agnew's scale to produce a new scale as depicted in Table 2 (also see Manatsa et al. 2007).

TABLE 2. Seasonal rainfall classification by EASR SPI value and corresponding event probabilities according to Agnew (1999). Note that 21% to 33.3% occurrence probability (in bold) has been added to the Agnew classification so as to accommodate the tercile (33.3%) method used in East Africa.

SPI value occurrence	Occurrence (%)	Nominal SPI class
>1.645	>=5	Extremely wet
1.282 to 1.644	6–10	Severely wet
0.842 to 1.281	11–20	Moderately wet
0.524 to 0.841	**21–33**	**Slightly wet**
−0.523 to 0.523	34–50	Normal
−0.841 to −0.524	**21–33**	**Slight drought**
−1.281 to −0.842	11–20	Moderate drought
−1.644 to −1.282	6–10	Severe drought
<−1.645	<=5	Extreme drought

3. Results

a. EOF analysis of equatorial East Africa short rains

It is evident from Fig. 1 that the topography of East Africa is complex; hence, the region is exposed to coastal and prominent topographic influences. Thus modulation of the rainfall is complicated by interactions of the near-surface flow with the complex topography. Because of this heterogeneity, it is not surprising that Mutai et al. (1998) noted the emergence of dramatic variations in climatological mean rainfall totals with seasonal rainfall anomalies tending to have coherence that is confined to small subregions. Some of the spatial coherence is generated by interaction of the large-scale regional atmospheric forcing with the topography. As such we expect large-scale atmospheric changes associated with, for example, IOD to have a stronger signal in the entire region. Therefore, in order to assess the spatiotemporal extent of this large-scale forcing, PCA was applied to the rainfall anomalies of the region. This domain-free technique enabled us to extract the dominant spatiotemporal characteristics of EASR for specified periods in this heterogeneous region. A scree test was used to retain the first four PCs as significant (Fig. 5).

PC1 explains by far the most of variability of EASR, accounting for more than 63% of the total variance. Thus in this work we concentrate on this first mode as a guide to approximate the general spatiotemporal variability of the dominant pattern of the regional rainfall. Since the main strategy is to determine the changes in the regional rainfall pattern, shifts in PC1 time series will be used to estimate the location of epochal change in the rainfall system. Figure 2 shows the temporal manifestation of the interannual variability of PC1 time series. Epochal patterns are quite distinct; these can readily be differentiated visually by the years 1918, 1961, and 1997 with the latest two periods displaying the highest amplitudes in the data record. No significant trend is evident in this PC time mode as indicated by the regression equation inserted in the figure. In any case, a search for shifts in the variance using the regime shift detector (Rodionov 2004) revealed significant shifts during the years 1961 and 1997. However, no significant change in the variance was realized during the year 1918 even though a conspicuously unique temporal variability pattern had been displayed during the period prior to this year. The broken line superimposed in Fig. 2 illustrates shifts in the PC1 variance as detected by the regime shift detector (Rodionov 2004) technique using the climatological period of 31 years as the cutoff length.

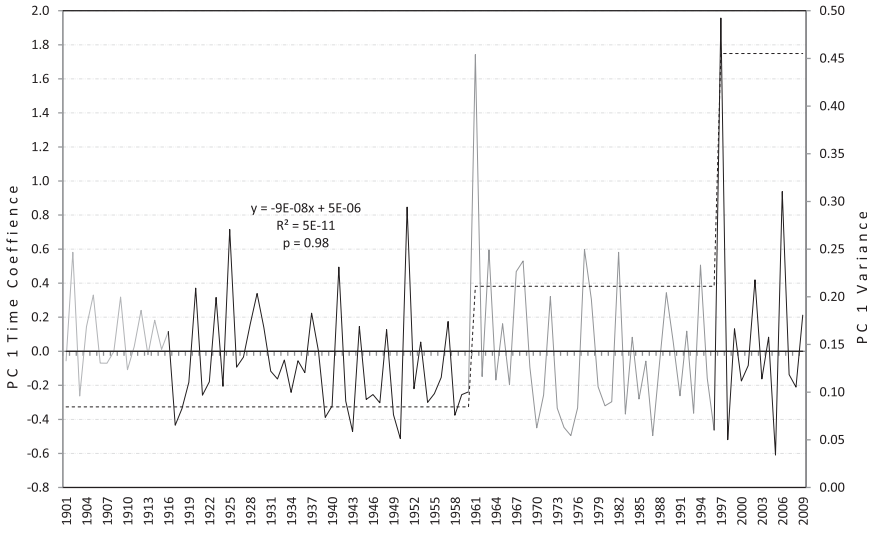

FIG. 2. Epochal manifestation of PC1 time series and its regression line (solid horizontal line next to the *x* axis). In the insert is the trend line equation. The broken line represents shifts in the variance as detected by the regime shift detector (Rodionov 2004).

The statistical results of the regime shift detector test are presented in Table 3. It can be noted that the first shift is more significant than the second shift, with *p* values of 0.002 and 0.076, respectively. This observation adds more evidence toward the physical existence of shifts of climatological significance during at least the two periods of 1961 and 1997. However, a test for the shift in the mean using the same technique did not yield any significant change in this parameter.

To ascertain how these shifts could have interfered with the variance of the EASR explained by PC1 time series, we subjected the two time series to running correlation analysis. In this way the temporal changes in the representativeness of the time coefficient of the EOF1 to the actual regional rainfall variability can be deduced. In Fig. 3 we show the running correlation using the climatological period of 31-yr segments. Here the correlation coefficients increase from 1948 to 1951 after a prior falling trend. The relationship then increases even more abruptly around 1961 before decreasing swiftly in 1990. An abrupt rise ensures again after 1996. It is interesting to note that the link between PC1 time series and EASR increased drastically in single-year periods, first in 1961, after consistently lower values in the earlier decade, and in 1997, also after more than half a decade of a relatively weakened relationship. In this way Fig. 3 confirms the existence of the two years as periods when significant changes took place in the relationship. Thus, we conclude that either a new (preexisting) dominant rainfall controlling mode is triggered (enhanced) in 1961 before abruptly but temporarily subsiding in influence around 1990 and is finally activated abruptly again from 1997.

The realization that the years 1918, 1961, and 1997 are important turning points within the dataset prompted us to examine the behavior of the first four PCs, initially for the entire duration and later for the epochs as demarcated by the three turning points. In Fig. 4 we present the cumulative variances (%) of the four loading components for each epoch including the entire duration. From this figure we can see that the first EOF component significantly varies within the demarcated epoch and contributes a minimum of 48% to the total variance in each epoch. In fact, of the four loading components presented, EOF1 is the mode with the most interesting and unique temporal character. This first mode has a continuously increasing trend of explained variance within the demarcated epochs. This indicates that the rainfall variability over East Africa is being influenced from a source that is increasingly becoming stronger within the defined epochs. No definite systematic trends can easily be determined from the other EOF modes. This implies that an important rainfall triggering mechanism of the rainfall of East Africa should have significantly developed or strengthened within the given epochs, principally through altering PC1 in epochs. Given that PC1 explains a reasonably large fraction of the rainfall

TABLE 3. Detected shifts in the PC1 time coefficient variance using the software designed by Rodionov (2004) when the climatological period is set as the cutoff length (L = 31 yr).

Shift year	Duration before shift	Variance after/before shift (Diff)	CSSI	*P* value
1961	60 yr	0.085/0.211 (0.126)	0.104	0.002
1997	36 yr	0.211/0.455 (0.244)	0.003	0.076

FIG. 3. The 31-yr running correlation between EASR and its PC1. Values are at the end of the 31-yr segment.

variance, especially in the later epochs, it becomes logical to dwell more on PC1 characteristics when making generalized statements about the changing nature of East African rainfall variability.

The increasing variance explained by PC1 in each succeeding epoch in Fig. 4 should reflect the stronger temporal control of the rainfall processes over East Africa. In other words, this is a manifestation of the region's epochal loss of the finer-scale structure in the rainfall triggering mechanisms as the integration moves toward a more organized and coherent state. It is apparent that this may not be an artifact of direct global warming impact as the change is initiated not only swiftly but in phases also. The sudden change started with 1918 and upgraded in 1961 before being further enhanced in 1997. The interpretation is that, with the phase progression in the epochs, fewer modes are correspondingly needed to represent the main features of the rainfall variability of East Africa. In such a case, it could be interesting to investigate the spatial coherence of this PC1 as determined by each epoch. This may assist in identifying the possible climatic mechanisms responsible for developing the related spatial signature over the region.

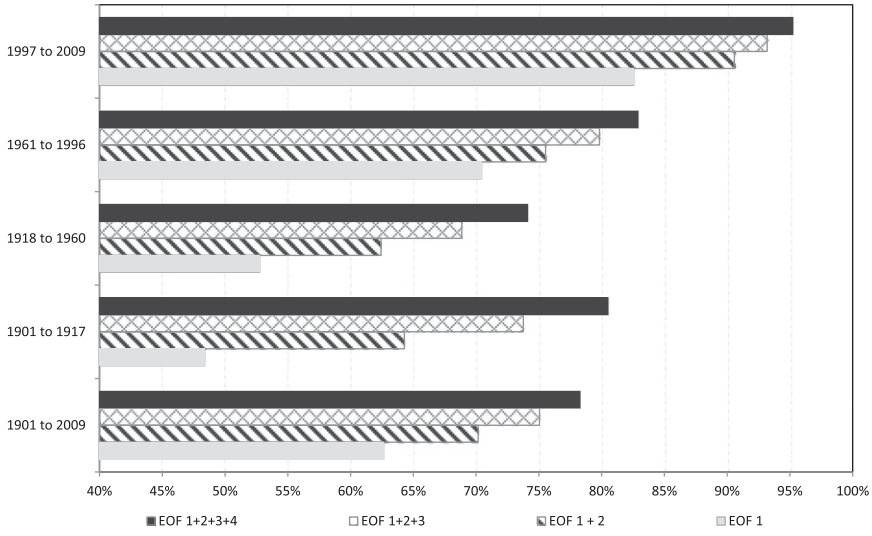

FIG. 4. Cumulative variance of the first four PCs for the entire period and the four epochs.

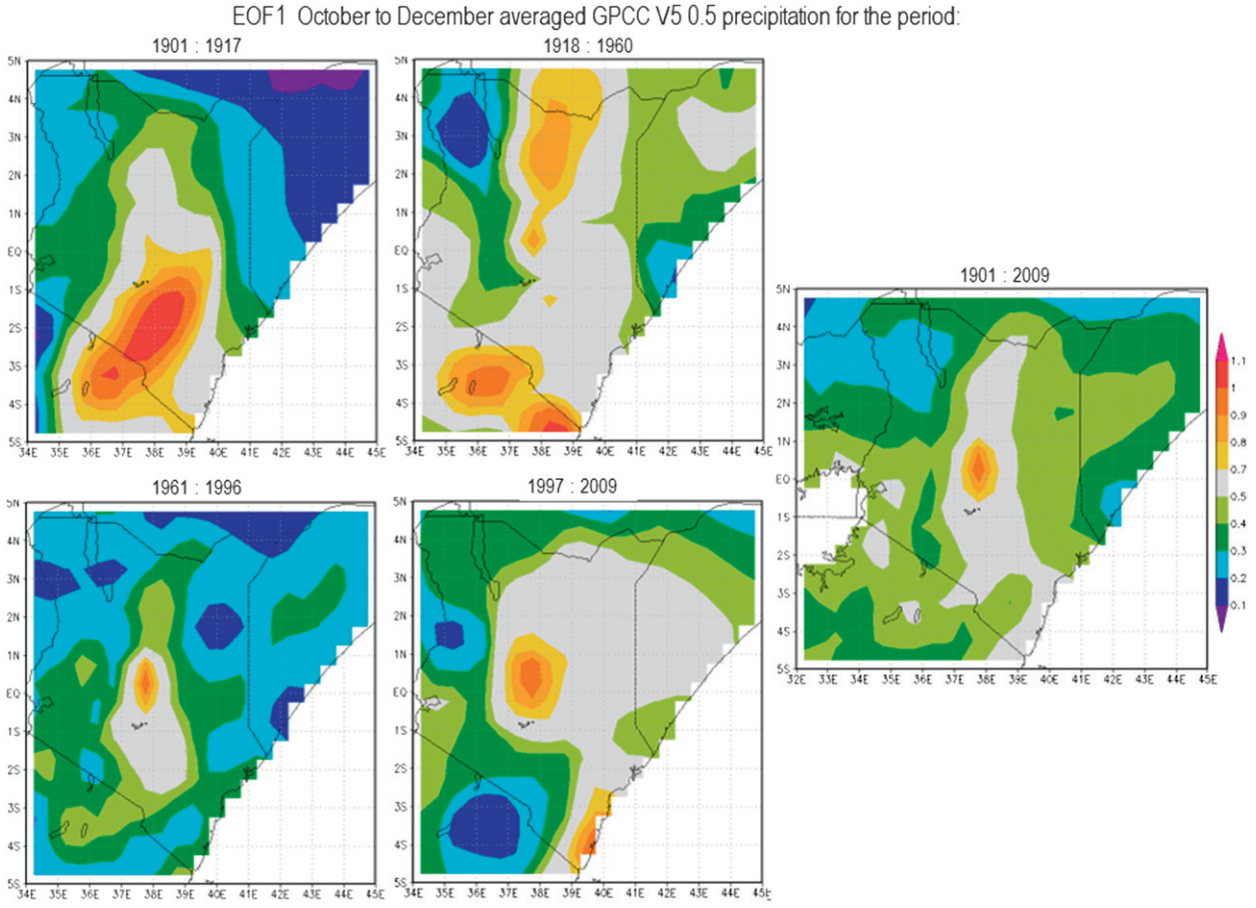

FIG. 5. Spatial coherence of PC1 for the epochs 1901–17, 1918–60, 1961–96, 1997–2009, and 1901–2009 for equatorial East Africa.

Figure 5 displays the spatial distribution of the PC1 for each of the four epochs including the whole period. All the spatial loadings for these dominant PC exhibit consistently positive values throughout the epochs. This predominantly monopole distribution of the spatial loadings indicates that the EASR essentially varies in a similar phase throughout the region in all the epochs. Thus during the averaged OND season, droughts and floods (positive and negative rainfall anomalies) are expected to generally cut across the whole region simultaneously, although obviously intensities may differ from place to place. However, the notable differences that are conspicuous in the spatial patterns reflect the changing nature of the underlying rainfall generating processes over the region. This may become clearer as we discuss the rainfall triggering mechanisms for each epoch in later sections.

The variation in the epochal spatial structure depicted in Fig. 5 makes sense if one considers that the rainfall mechanisms are largely a result of the combination of uplift by convection and action of relief on the prevailing wind. As such, PC1 for the first to the third epoch has a strong meridional orientation that principally reflects the spatial coherence of the rainfall due to uplift by the underlying land surface (e.g., topography) and surface wind with considerable meridional component from the southern coast. This is mostly because the highlands of the region are situated in the high-value area of the first component distribution map, with isolines higher than 0.9 almost reflecting the areas of high relief trend in these regions. Hence, despite the intensity, these epochs are mostly representative of the rainfall variability whose cohesiveness is principally dominated by topography and meridional wind.

However, PC1 for the second epoch has more localized structures that are also scattered with no recognizable pattern over the region. Since more modes are necessary to represent the smaller-scale variations, this could explain why the cumulative variance explained by the four modes is the least relative to other epochs. In contrast, the last epoch has the greatest spatial coherence of PC1 with limited localized features. As such,

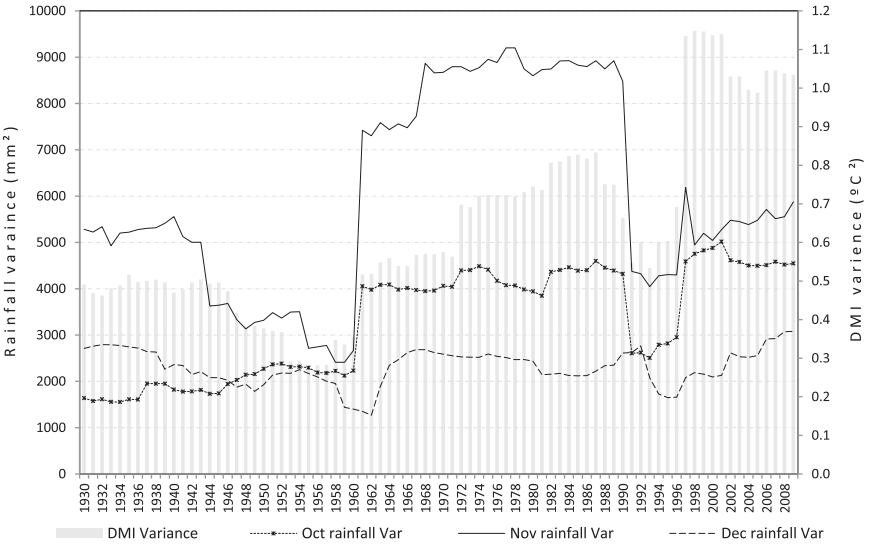

FIG. 6. The 31-yr moving monthly rainfall variance for equatorial East Africa. Bars represent the DMI variance. Values are at the end of the 31-yr segment.

the rainfall-related mechanisms responsible for last epoch are so overwhelming in the region that they do not only simplify the spatial structure of the rainfall field but also increase its coherence on the spatial scale. Hence PC1 tends to explain an incredible 83% of the region's rainfall variation. It is interesting to note that this enhanced PC1 of the last epoch is remarkably tied to the western Indian Ocean as it displays a spatial pattern that is shaped by the 0.7 isoline that covers most of the interior and spreads to cover almost the entire coastline into the ocean. In the absence of clear-cut relief dependence in the last epoch, it is highly possible that this spatial structure is dominantly controlled by convection that originates from western equatorial IO. Thus we have linked epochal variations to possible rainfall triggering mechanisms. However, it has to be noted that the last epoch has the shortest time period and hence this limitation could also have impacted the interpretation of the EOF solutions.

b. The changing characteristics of EASR

The seasonal total that we have been analyzing may substantially conceal the finer details of the intraseasonal variability that could be responsible for the general alterations in the overall rainfall pattern. We therefore investigate separately the temporal nature of the three months that constitute the EASR. Although the Mann–Kendall test did not reveal any significant trend in the individual months, their 31-yr moving variances displayed quite varied decadal patterns (Fig. 6). However, these configurations bear very close resemblance to the one displayed by the dipole mode index (DMI; Fig. 6). A period of relatively low variability is evident before 1961, after which there is a sudden rise that then levels off until the early 1990s. Thereafter the activity subsides before taking yet another abrupt upward turn in 1997. Although the moving variances for individual months convey similar patterns, the magnitudes are correspondingly greatest for November and least for December. It has to be noted that while the post-1996 variance for the DMI is unprecedentedly high within its time series, rainfall variance is generally lower than its corresponding pre-1997 period values.

In Fig. 7 we demonstrate that the relationships of monthly rainfall show strong decadal variability. In this figure the two pairs of relationships that included the month of December only became significant after 1996. In fact, the rise to significance was abrupt, with the correlation between October and December (November and December) shooting from 1996 values of near zero (0.1) to about 0.6 in the following year. A similar abrupt shift in correlation has been experienced at an earlier stage between October and November rainfall where the correlation strengthened from 0.1 in 1960 to 0.6 in 1961. This demonstrates that the October rainfall became largely in phase with that of November from 1961 while December rainfall only became coupled to the variability of the other two from 1997. It has to be noted that there is a strong resemblance in this temporal correlation pattern between October and November and between PC1 and the EASR index (Fig. 4). Both processes reiterate the importance of the years 1961 and 1997 within the rainfall dataset.

This observation is further strengthened by the illustration in Fig. 7b where October and November rainfall

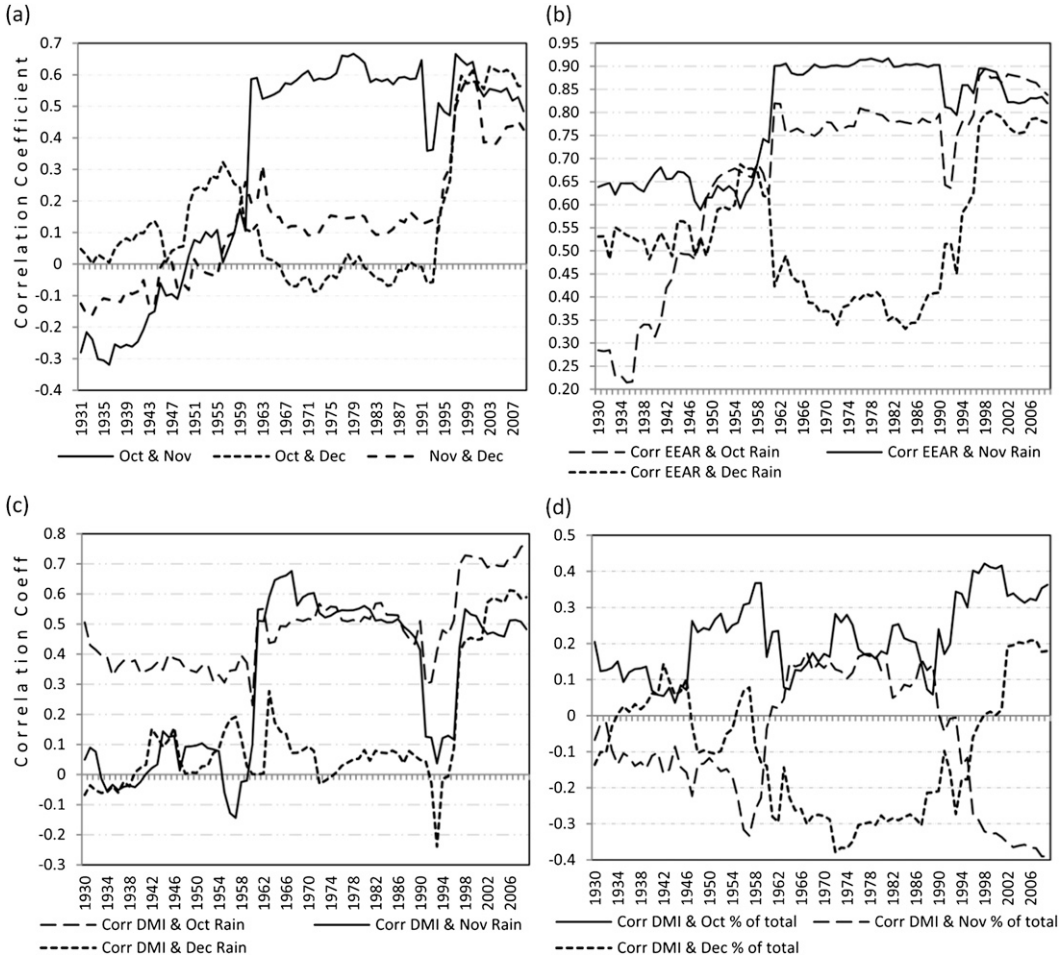

FIG. 7. The 31-yr moving correlation between the individual months of the OND season. Values are at the end of the 31-yr segment.

became more in phase with the seasonal rainfall index in 1961 whereas that of December became more strongly coupled after 1996. We also note that December rainfall became more linked to the seasonal rainfall index than the rest of the months from 1998. Thus the interannual variability of all the three months reverted to a predominantly in-phase mode after 1996. It is therefore most likely that a major rainfall transforming process brought the variability of October and November rainfall largely in phase from 1961 before all the months were concentrated by becoming strongly in phase from 1997.

The close similarities between the correlation patterns of the three monthly rainfalls with DMI presented in Fig. 7c suggest that the IOD is the most likely climate mode responsible for the noted variations in the rainfall variability. However, we note that despite the DMI becoming more significantly related to the rainfall index from 1961, the October rainfall was already consistently significantly correlated to the DMI prior to that period. Another interesting aspect is that after 1960 November rainfall had the strongest correlation average, which was significant, while December rainfall had the least, which was insignificant. But after 1998, October rainfall had the strongest correlation of 0.7, followed by that of December and November with 0.6 and 0.5, respectively. This demonstrates that significant changes have occurred at monthly time scales insofar as the influence of IOD on the rainfall season is concerned.

To shed more light on these alterations that occurred at monthly time scales, in Fig. 7d we present the correlation between the proportions of the monthly rainfall to the annual total with the DMI. Interestingly, for the three decades after 1960, there was significant negative correlation between the proportions of December rainfall to the total and DMI. This suggests that during lower (higher) values of DMI, the proportion of December rainfall total was higher (lower). However, after 1996

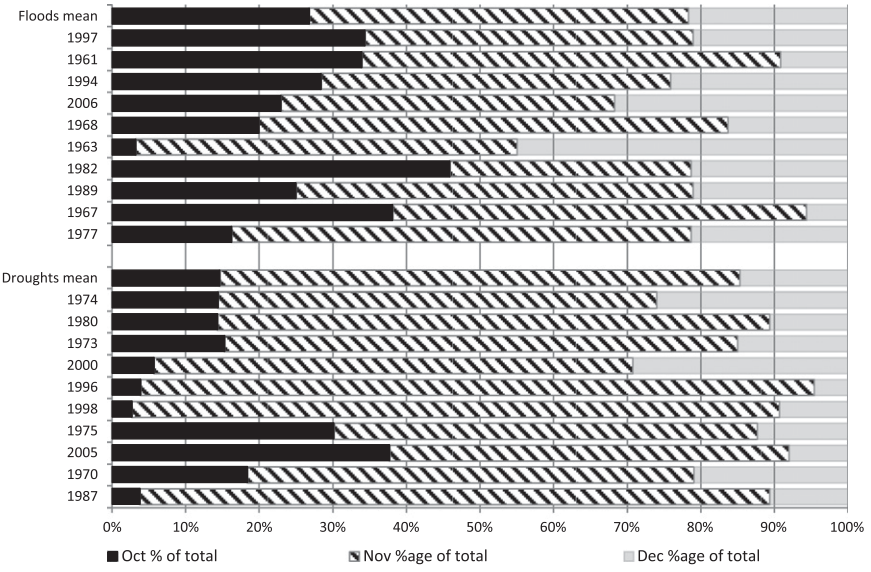

FIG. 8. The distribution of monthly total rainfall as a percentage of the seasonal total for the (bottom) ''drought'' and (top) ''flood'' composites and their constituent events. The years correspond to the 10 worst droughts (floods) in ascending (descending) order since 1901 with the most intense events at the bottom (top).

it was the proportion of the October and December rainfall that became more significant, with positive and negative correlation values respectively. Since higher (lower) values of DMI are related to surplus (deficit) rainfall, the implication in the post-1996 period is that the month of November may have a relatively bigger (smaller) proportion of the seasonal rainfall total during droughts (rainfall surpluses) compared to other years. On the other hand, October may comparatively have a reduced (increased) percentage of the seasonal total during droughts (floods).

We explained this observation by first selecting extreme rainfall years using the EASR SPI values of ± 0.84 as the threshold level (see Table 2). These years are presented in Fig. 8 together with the monthly contribution to the seasonal total. The rainfall events correspond to the 10 worst droughts (floods) in ascending (descending) order since 1901 with the most intense at the bottom (top). Although the events have been selected from the period from the beginning of the twentieth century, they all fall within the period from 1961. In this figure we refer to the positive years as ''floods'' and negative years as ''droughts.'' In the drought composite the October percentage is relatively low (averaging 14%) while that of November is relatively high (averaging 71%). On the other hand, in the flood composite October has a mean percentage of 27%, which is almost twice as much, and November has 50%, which is a reduction of about a third of its flood composite value. This interesting pattern is reflected more vividly in the worst drought of 1987 where November contributed the largest percentage to the seasonal total while October had the least during the study period. On the other hand, in the scenario of the worst floods of 1997, November and October contributions to the total were among the least and largest, respectively. However, December does not show much variation within these composites as it has an average of 15% for droughts and 20% for the flood composite.

These observations demonstrate that although November is the core of the rainfall season with the greatest percentage, its rainfall amount counts more during the droughts where its proportion of the seasonal total is greatest. During surplus rainfall, the other months cut into the proportion of the November total, making the distribution relatively less skewed. The implication is that during droughts, rainfall conservation measures should be maximized during the period of November as this month may still have rainfall amounts that may not deviate significantly from the norm. At the same time, early cessation and late onset of the season is more likely. Since the described pattern has been observed to be more pronounced in the post-1996 period, it bears testimony to the changing intraseasonal rainfall variability of the short rains on monthly time scales. The significant correlation with DMI during this period signifies the importance of the IOD events not only to increased extreme events, but to the modulation of the rainfall on monthly time scales as well.

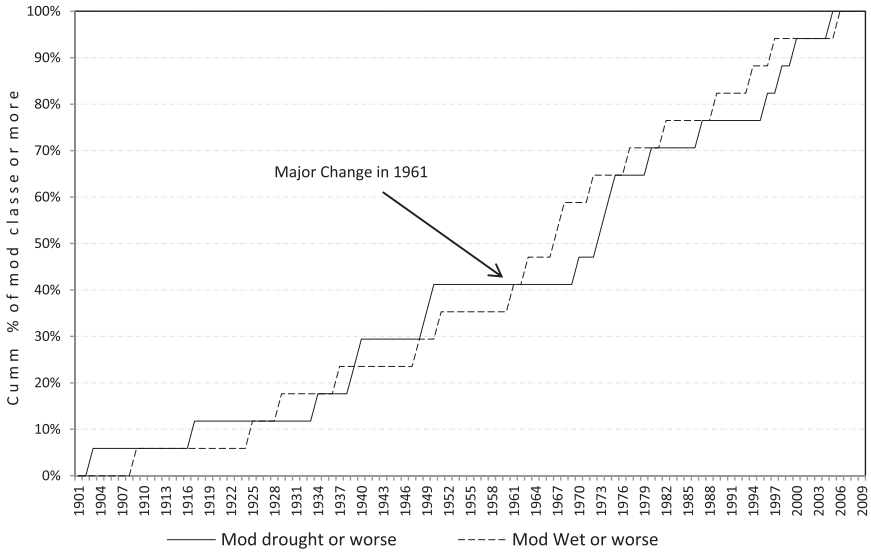

FIG. 9. Cumulative distribution of EASR SPI with moderate or more intense classes.

In any case, in the absence of a clear tendency in both the monthly and seasonal rainfall time series, but with dry and wet episodes in the region becoming longer and more intense, it should follow that the rainfall amount and intensity in the wet season may have increasing trends. We therefore adopt for use the SPI technique. This method allows for a more detailed monitoring of dry and wet periods over a wide spectrum of temporal scales (Edwards and McKee 1997) since it is able to return fundamental parameters in the analysis of the occurrence of different wet/drought types in terms of severity, magnitude, and frequency. In the SPI analysis we adopted the seasonal scale of the corresponding three months. Figure 9 displays the cumulative distribution of the EASR SPI classes of moderate intensity or more. It can be noted that more than 65% of the wet events of moderate class or more occurred after the 1950s; similarly, about 59% of the dry events occurred after 1969. There were prolonged periods during the earlier decades of the century when there was either no drought or wet episodes. For example, no drought event of moderate class or more occurred during the two decades from 1950 to 1970 and only two such events occurred in the first three decades of the century. Although such a scenario is less pronounced in the wet events, we also note that only one event of moderately wet class or more occurred within the first two and a half decades of the twentieth century. This is a clear indication of more extreme events being located within the later decades of the study period. In fact, the relative frequencies of these wet and dry episodes changed significantly as from 1961. During this year, the frequency of occurrence of wet incidences became predominantly higher than that of the dry occurrences, with the moderately wet or worse classes assuming unprecedentedly greater and consistent nature of occurrence than their opposite counterparts.

To derive a more detailed illustration of how more extreme EASR SPI classes are distributed, we present a similar graph in Fig. 10 that better illustrates more intense events of severe class (or worse). It is noted that the distribution of the severely wet/dry conditions is even more skewed to the left with more extremes of this nature located within the second half of the study period. Two extended periods of the severely wet conditions or worse classes occurring almost in succession are apparent in the post-1949 period. It is in this era that 86% of these excessive rainfall events are located with an equal distribution of 43% each within the two periods, 1960 to 1968 and 1993 to 2006. These two epochs are unique in the sense that they do not only display exceptionally prolonged phases of very wet conditions during the study period, but they also have the wettest rainfall events occurring in 1961 and 1997. Coincidentally, these two events were years when the IOD had its greatest east–west SST gradient since the late 1890s. This provides more rooted evidence that it is the behavior of the IOD that should explain better the development of these extreme wet events. However, dry episodes of similarly high intensities are relatively less skewed to the left, with 60% of the severe droughts or worse occurring after 1968. It is the severely wet conditions or worse that are more sensitive to the 1961 period than the SPI classes of severe deficits or worse. This means that the triggering mechanisms for more intense events had greater impact on the rainfall

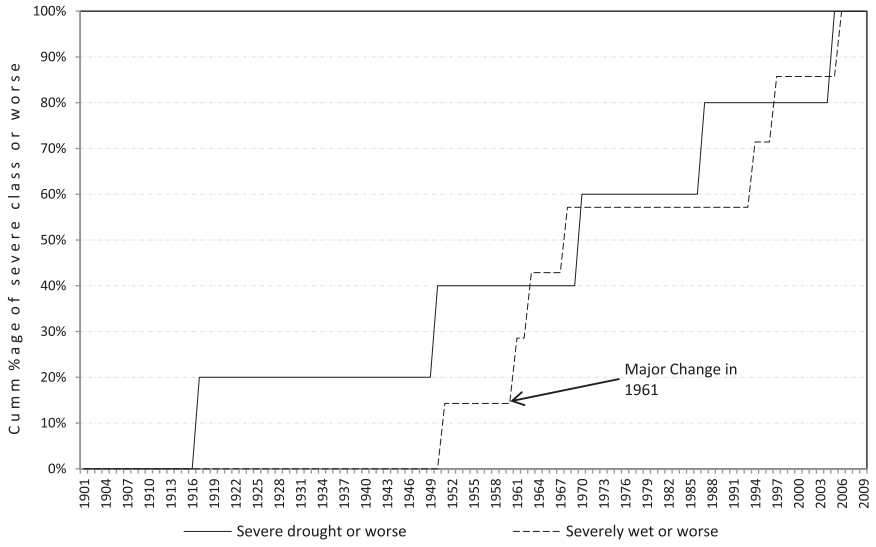

FIG. 10. Temporal distribution of the rainfall events that are severe or worse.

surpluses than on the deficits, especially in the decades from the 1960s to mid-1990s.

c. *Impacts of shifts in IOD on EASR SPI*

A simple correlation analysis performed between EASR SPI and the dipole mode index time series from 1901 to 2009 yields an overall negative value of −0.53, which is significant above the 99% confidence level. But when the relationship is subjected to 31-yr segments of the study period, epochs emerge where the correlation is insignificant for the period up to the early 1960s whereas it is notably altered in the mid to late 1990s. In fact, when separately correlated to the SST anomalies of the IOD poles, different patterns emerge (see Fig. 11). It is noted that the most consistently significant correlation is between the SSTs of the eastern pole and the EASR while the least reliable link is between the EASR and the SST anomalies of the western pole.

The temporal manifestations of the 31-yr running variances of the three time series also show the close

FIG. 11. Temporal manifestation of the 31-yr running correlation coefficients among EASR, DMI, and SST anomalies of the western IOD pole.

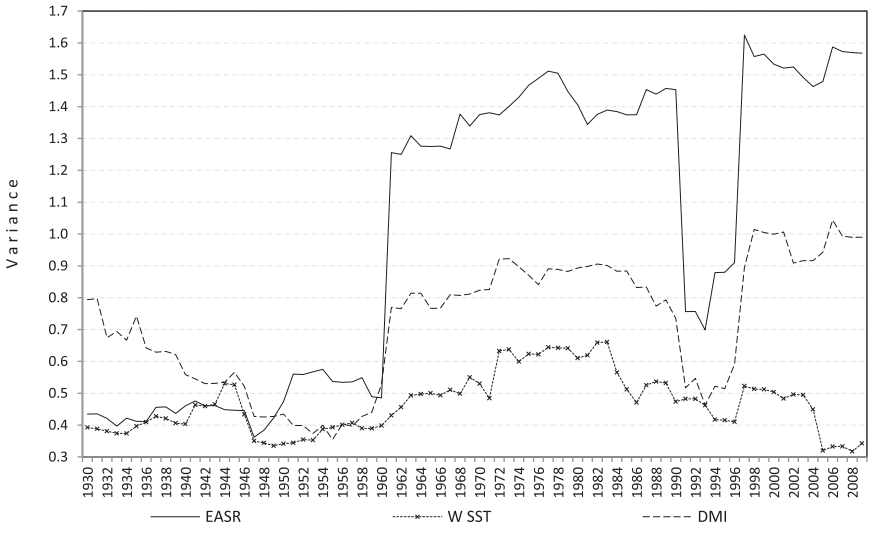

FIG. 12. The 31-yr running variances for EASR SPI, W SST, and DMI time series. Values are at the end of the 31-yr segment.

relationship between the pattern depicted by the EASR SPI and DMI (Fig. 12). Although all running correlations are sensitive to the 1997 shift, only that of the DMI and EASR SPI shows a swift transition in 1961. The observation gives us a clue that it may not have been the rising temperatures in the western pole that brought about the observed changes in the regional rainfall extremes as postulated by Nakamura et al. (2009). Rather it is the DMI's association with the EASR through the temporal coupling between the two subsystems that clearly brings about the identified shift points of 1961 and 1997. Therefore, it is most likely that the latter two shift points in the rainfall variability are more related to the IOD process in its entirety than to its individual east and west SST anomaly components.

Given that the IOD has been known to be characterized by epochs demarcated by the shift points of 1918, 1961, and 1997 (Manatsa et al. 2012), we therefore hypothesize that it is these turning points that shape the noted changing characteristics of the EASR SPI classes since the turn of the twentieth century. The scatter diagram (Fig. 13) illustrates better the changing nature of the epochal relationships between DMI and EASR SPI as demarcated by the mentioned three shifts. Here

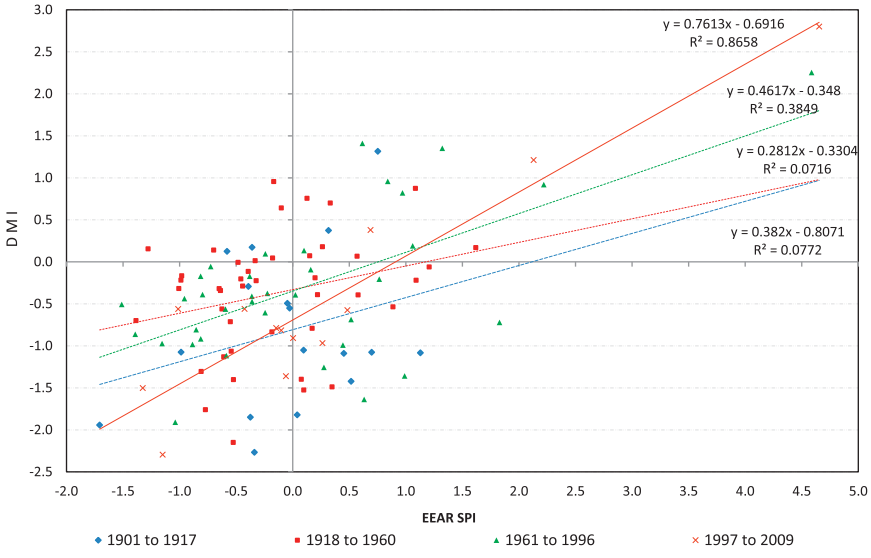

FIG. 13. Scatterplot of EASR SPI against the DMI relative to the IOD epochs. In the insert are regression lines and corresponding regression equations for each epoch in ascending order.

TABLE 4. Contingency table for observed frequencies of EASR SPI classes and IOD epochs.

IOD epoch	Extremely wet	Sevevely wet	Moderately wet	Slightly wet	Normal	Slightly dry	Moderately dry	Severely dry	Extremely dry	Total
1900–17	0(0.95)	0(0.16)	1(1.40)	2(1.25)	11(7.80)	1(2.81)	1(1.87)	0(0.62)	1(0.16)	17
1918–60	1(2.37)	0(0.39)	4(3.55)	2(3.16)	20(19.73)	11(7.10)	4(4.73)	1(1.58)	0(0.39)	43
1961–96	3(1.98)	1(0.33)	4(2.97)	3(2.64)	12(16.51)	6(5.95)	5(3.96)	2(1.32)	0(0.33)	36
1997–2009	2(0.72)	0(0.12)	0(1.07)	1(0.95)	7(5.96)	0(2.15)	2(1.43)	1(0.48)	0(0.12)	13
Total	6	1	9	8	50	18	12	4	*1*	109
Df = 24			$\chi^2 = 25.481$			P value < 0.0001				

it is noted that the linear relationships have only became significant in the third epoch and even stronger in the last epoch. This hypothesis can be strengthened by using the chi-square (χ^2) test for testing the independence of the two attributes, the IOD epochs and the EASR SPI classes. This is examined in the following section.

d. Chi-square (χ^2) test of significance between EASR SPI and IOD epochs

Since the χ^2 uses the data that have been expressed in frequencies, it was necessary to first put the frequency of the EASR SPI classes into the four DMI categories. Based on these categories, a contingency table for the observed frequencies was prepared as shown in Table 4. From these observed frequencies, expected frequencies and the χ^2 value were computed by the usual procedure. In the contingency table provided in Table 4, the null hypothesis was that there is no relationship between the two variables (i.e., the expected values in the rows and columns are independent). An analysis of the table shows that the χ^2 for the rainfall frequencies is 26.38, with a p value of 0.0017. In this way, the null hypothesis of no relationship has to be rejected in favor of the existence of a strong dependence of the SPI classes on the epochs. This implies that on more than 99.9% of the occasions, there is the likelihood that the frequency of the EASR SPI classes is determined by the epoch in which they occur. Thus, the demarcation of EASR based on the four epochs is realistic in both a physical and statistical sense, and not a direct consequence of the application of the statistical techniques.

Having established the statistical significance of the relationship between the SPI classes and the IOD epochs, we go further to illustrate more clearly in Fig. 14 how the EASR SPI classes are distributed within the epochs. The general trend from this figure is that the percentage of normal rainfall in each epoch is generally decreasing in each progressive epoch at the expense of increasing rainfall extremes. The SPI classes were more in the normal categories but became reduced toward the third epoch where the graph flattens as more extreme events classes become more prevalent. We may not conclusively explain events over the last epoch because it is still of indeterminate length. However, the epoch has already recorded a fair share of extreme rainfall events at the expense of normal rainfall events. Thus, although there were no long-term trends of the short rainfall anomalies, rainfall variability in East Africa may have experienced

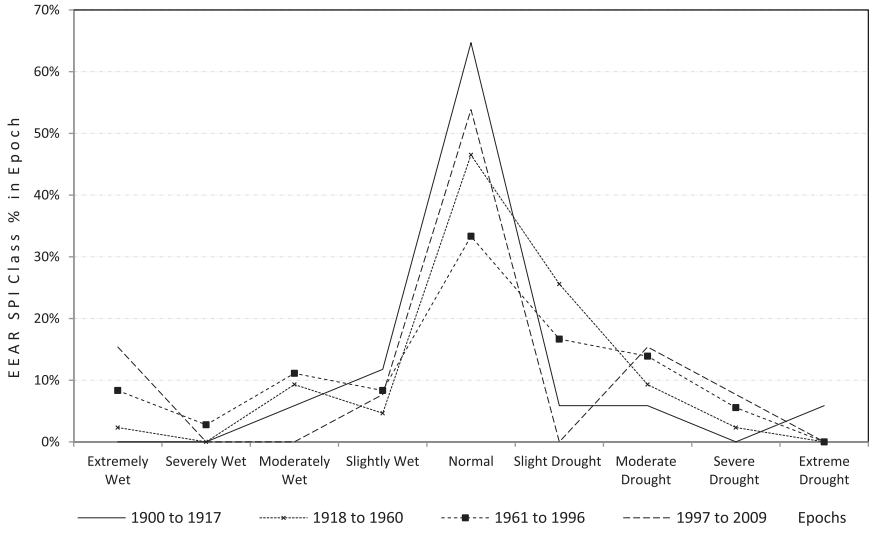

FIG. 14. Distribution of EASR SPI classes according to the four IOD epochs.

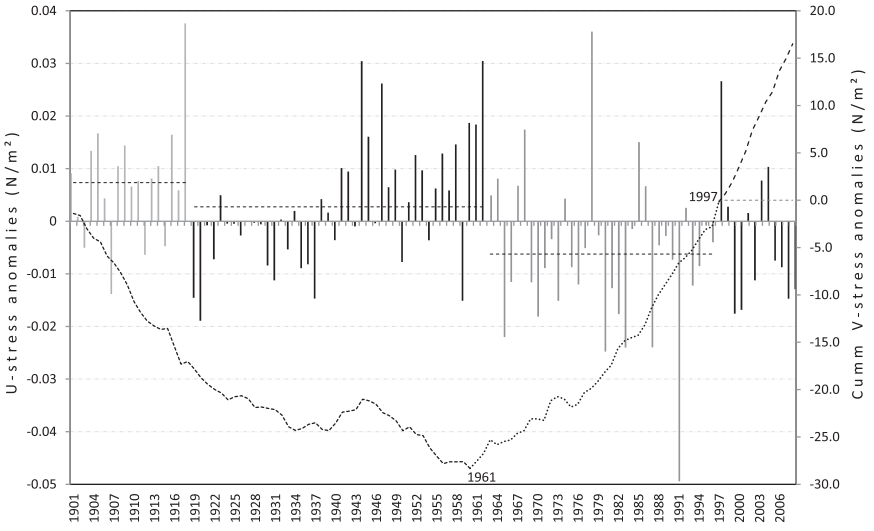

FIG. 15. Temporal manifestation of the eastern pole's zonal wind stress anomalies ($N\,m^{-2}$) alongside its cumulative values. In the insert are the years depicting the turning point of the cumulative graph and broken lines indicating the average wind stress values for each epoch.

significant IOD-induced modulations, especially in recent decades. In particular, because of the recently established high spatial cohesiveness of the regional rainfall, droughts and floods have not only become more intense but also more widespread.

e. The nature of the relationship between the IOD events and EASR SPI

It is expected that the discontinuities in the DMI, which define the epoch demarcations in the IOD, should also be visible in the surface zonal wind of the tropical SIO. In the light of this realization in Fig. 15 we present the interannual zonal wind stress anomalies extracted from the western IOD pole but south of the equator, alongside their cumulative temporal pattern. It can be appreciated that the wind stress anomaly values decrease from the first to the second epoch before reversing to negative. An increase in magnitude is then witnessed from the third to the fourth epoch. However, the most intriguing aspect of this analysis is demonstrated in the cumulative graph. Here we note that the cumulative pattern of the wind stress anomalies does not

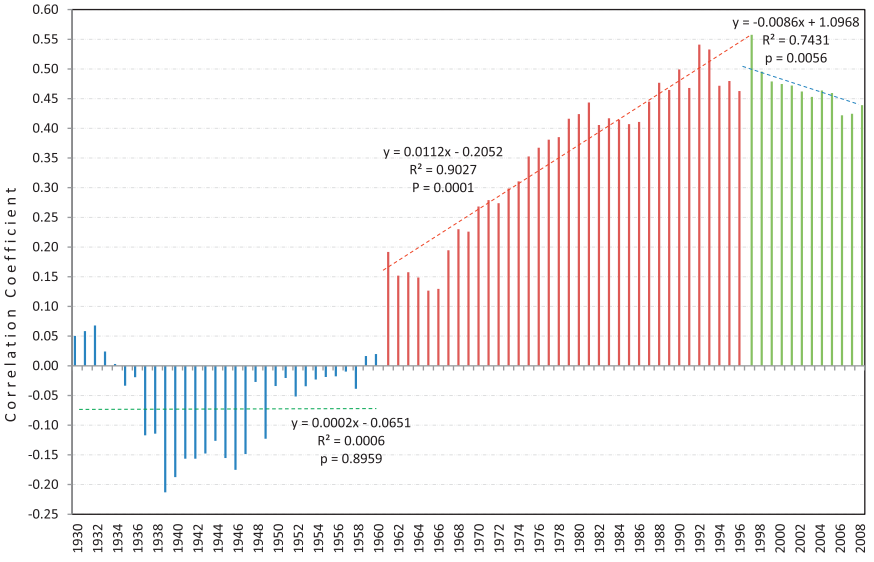

FIG. 16. Temporal patterns of the 31-yr moving correlation coefficients between EASR SPI and *u*-wind stress for the western pole of the IOD. In the insert are the regression lines together with their corresponding equations for the correlation values.

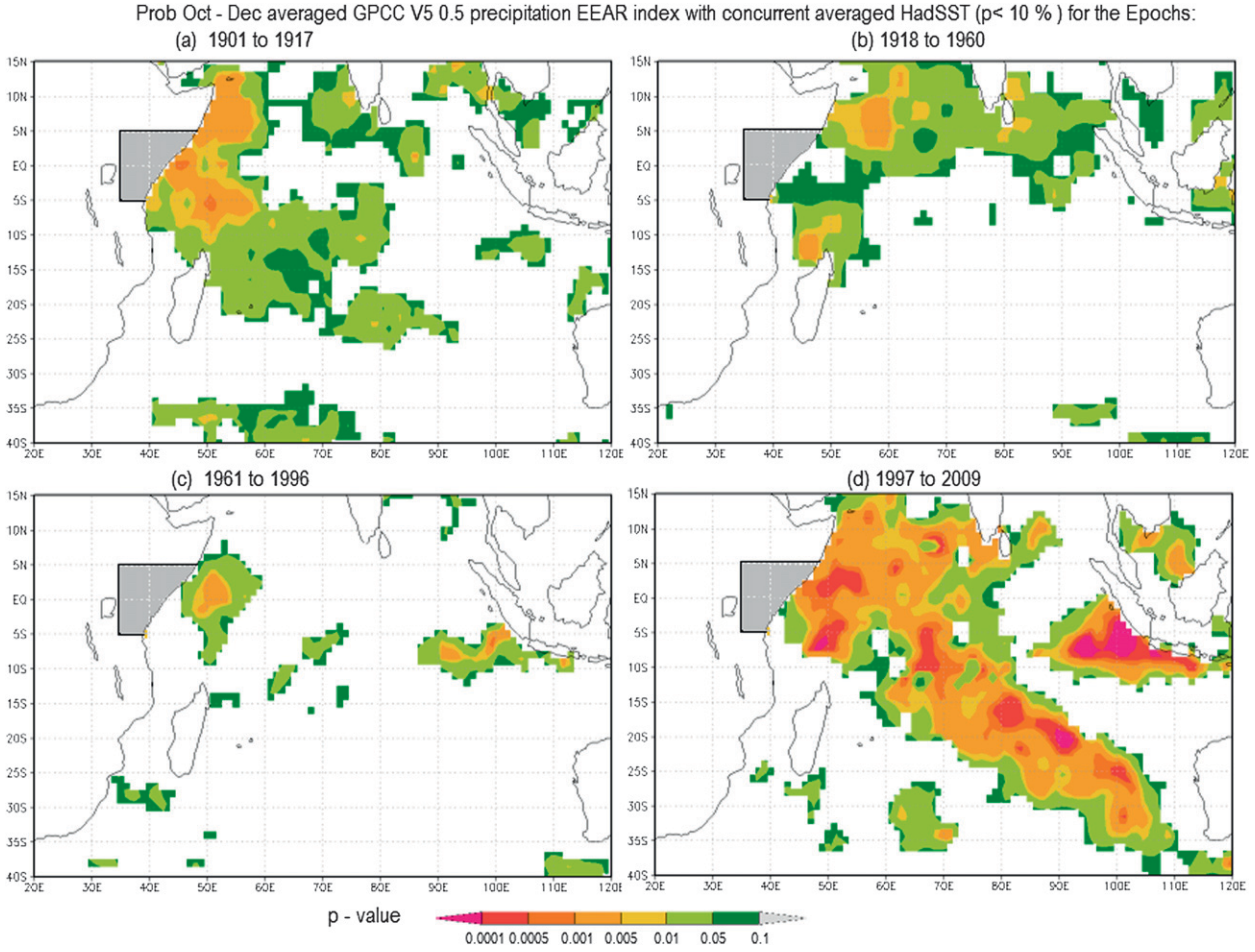

FIG. 17. The *P* values for the epochal correlation fields between EASR and SSTs for the Indian Ocean for (a) 1901–17, (b) 1918–60, (c) 1961–96, and (d) 1997–2009. The shaded region over East Africa is the area for the averaged EASR index.

only reverse gradient in 1961 but surprisingly changes sign from negative to positive in 1997. For this reason, we can conclude that the circulation pattern over the western pole also carries with it information about the major turning points in the IOD system through the wind stress.

Furthermore, a striking temporal correlation pattern emerges in Fig. 16 where we correlated EASR SPI with the *u*-wind stress using 31-yr running segments. Although initially insignificant, the correlation coefficient values reversed from being negative to positive around 1961. Once the positive values were initiated, they continued with a significant increasing trend until 1997, when the values began to fall gradually with a significant negative trend. It is therefore more likely that the zonal wind variability played a significant role in the changes identified in the EASR SPI classes. It is when the zonal winds started to have a strong enough easterly anomaly that the IOD began to have a significant impact on EASR; this coincided with the IOD shift of 1961. Easterly anomalies in surface winds have been known to reduce the normal moisture transport away from East Africa (e.g., Mapande and Reason 2005), thereby creating conditions conducive for rainfall development.

f. Impacts of IOD on EASR SPI

Having established the strong coupling between EASR SPI and zonal wind component over the western pole and the less significant role of the underlying SST anomalies, we move on to investigate how the IOD is actually linked to the regional rainfall. An investigation to characterize the correlation of the EASR with the Indian Ocean SST field reveals a dipole configuration that is reminiscent of the IOD mode captured only in the third and fourth epochs of Fig. 17. It is therefore evident from this figure that interannual fluctuations in East African short rains became more closely tied to the large-scale atmospheric circulation through the anomalously warm

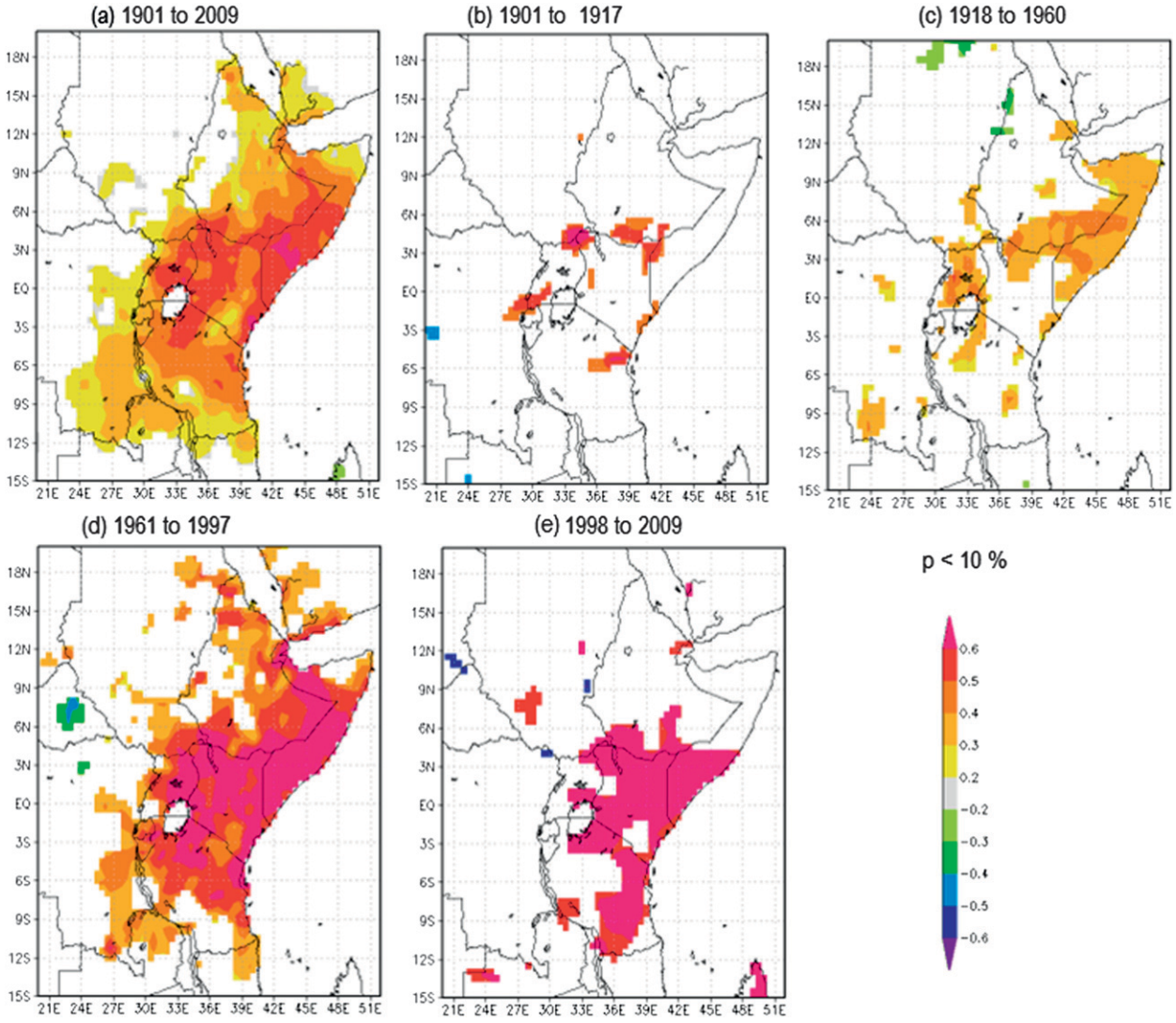

FIG. 18. Correlation field of the DMI with the GPCC precipitation field ($p < 10\%$) over the northeastern region of Africa for the periods (a) 1901–2009, (b) 1901–17, (c) 1918–60, (d) 1961–96, and (e) 1997–2009.

and cold SSTs in the western and eastern part of the Indian Ocean domain as from 1961. While it appears in the third epoch that the EASR was linked solely to SST anomalies of the two poles, there is an additional dimension of the region with a southeast–northwest diagonal orientation toward East Africa in the IO during the last epoch. This attaches an equally important simultaneous influence of the southeast trade winds variability to the IOD impacts on EASR in the last epoch. This is in contrast to the first epoch where the region of significant correlation is linked to the diagonal orientation but not to the IOD pattern. The second epoch has the significant region of association restricted mainly to the north of the equator with neither an exclusively defined IOD pattern nor a southeast–northwest orientation. It shows, despite demonstrating that the IOD SST pattern became significantly linked to EASR after 1960, that there was an additional trade wind variability influence after 1996.

Further investigations of the impact of DMI on the whole region of East Africa are presented in Fig. 18. This figure reveals that the influence was insignificant in the first epoch, confined mainly to the horn of East Africa in the second epoch, widespread to most of the region west of 30°E in the third epoch, and mostly restricted to the central coastal regions in the last epoch. This observation demonstrates the epochal nature of the IOD influence over East Africa by indicating that the impact became established over equatorial East Africa only after 1960 before being more focused on the equatorial

coastal regions in the last epoch. Thus, IOD influence on the East African region varies not only in space but also with time as determined by the epochs.

4. Summary and conclusions

The rain gauge–based GPCC monthly precipitation dataset for the period 1901 to 2009 is used to demonstrate the existence of the epochal changes in the EASR. We noted, through the temporal distribution of the EASR event classes determined by the SPI technique, that the EASR has intensified significantly from the turn of the twentieth century, with more floods and droughts occurring in the recent decades. This increase toward more extreme rainfall events has not been gradual but is strongly characterized by epochs dictated by shifts in the Indian Ocean dipole (IOD) mode. These shifts occurred during 1961 and 1997. The shifts were also quite prominent in the NCEP–NCAR wind data from the western pole of the IOD mode. The periods around 1961 and 1997 have already been confirmed as times when real shifts occurred in the Indian Ocean as seen from the IOD time series (Manatsa et al. 2012), coral records (Nakamura et al. 2009), and stable isotopes (Vuille et al. 2005).

Before 1961 no significant connection could be derived between the IOD and the EASR. However, a relatively strong coupling between the two occurred almost instantly in 1961 and thereafter until 1997, when another abrupt shift in correlation occurred to even stronger coupling. The PC1 extracted from the EASR spatial domain initially explained just about 50% of the rainfall variability before 1961, and then catapulted to about 73% between 1961 and 1997, before eventually shifting to exceed 82% after 1997. The PC1 for each successive epoch also displayed loadings with notably improved spatial coherence. This systematic pattern of increase was accompanied by both a sharp increase in the frequency of rainfall extremes and spatial coherence of the rainfall events over the region. Thus, the epochal shifts may also explain why rainfall extremes undertook an upsurge turn after every shift with the corresponding increased coupling between IOD and the rainfall. Hence, it is most likely that the 1961 and 1997 IOD shifts are responsible for the epochal modulation of the EASR in both the spatial and temporal domain.

But the observed epochal changes in IOD attributes such as its variance and its relationship with EASR appear in this work to be a system-wide phenomenon that is yet to be comprehensively understood. However, this epochal variation or apparent nonstationary nature in the IOD–EASR relationship is novel and has rarely been considered by recent researchers. Yet epochal shifts, if not recognized in a timely way, can undermine statistical prediction schemes that are based on stationarity relationships in historical data. This study revealed that EASR variability was relatively constrained in the earlier decades when the IO SSTs were cooler but increased significantly in the recent decades as the SSTs warmed considerably. These findings support the notion of greater climate variability tending to develop in warmer climate states. This inference fits the growing consensus that the current global warming will eventually increase the frequency of extreme rainfall events. Hence climate change impacts will bring further environmental stress to the region of East Africa, which already has a reduced capacity to adapt to the mounting adverse effects of the current smaller-scale climate variability.

Acknowledgments. JAMSTEC is acknowledged for providing the sponsorship and research facilities for this work. We appreciate Bindura University for providing partial funding. The first author was supported by a RONPANKU scholarship.

REFERENCES

Abram, N. J., M. K. Gagan, J. E. Cole, W. S. Hantoro, and M. Mudelsee, 2008: Recent intensification of tropical climate variability in the Indian Ocean. *Nat. Geosci.,* **1,** 849–853, doi:10.1038/ngeo357.

Agnew, C. T., 1999: Using the SPI to identify drought. *Drought Network News,* **12,** 6–12.

Annamalai, H., S. P. Xie, J. P. McCreary, and R. Murtugudde, 2005: Impact of Indian Ocean sea surface temperature on developing El Niño. *J. Climate,* **18,** 302–319.

Behera, S. K., J. J. Luo, S. Masson, P. Delecluse, S. Gualdi, A. Navarra, and T. Yamagata, 2005: Paramount impact of the Indian Ocean dipole on the East Africa short rains: A CGCM study. *J. Climate,* **18,** 4514–4530.

Black, E., J. Slingo, and K. R. Sperber, 2003: An observational study of the relationship between excessively strong short rains in coastal East Africa and Indian Ocean SST. *Mon. Wea. Rev.,* **131,** 74–94.

Breaker, L. C., 2007: A closer look at regime shifts based on coastal observations along the eastern boundary of the North Pacific. *Cont. Shelf Res.,* **27,** 2250–2277, doi:10.1016/j.csr.2007.05.018.

Clark, C. O., P. J. Webster, and J. E. Cole, 2003: Interdecadal variability of the relationship between the Indian Ocean zonal mode and East African coastal rainfall anomalies. *J. Climate,* **16,** 548–554.

Dionne, G., P. Francois, and O. Maalaoui, 2009: Detecting regime shifts in corporate credit spreads. CIRPÉE Working Paper 09-29, 44 pp. [Available online at https://depot.erudit.org/id/003093dd.]

Edwards, D. C., and T. B. McKee, 1997: Characteristics of 20th century drought in the United States at multiple timescales. Colorado State University Climatology Rep. 97–2, Atmospheric Science Paper 634, 155 pp.

Figura, S., D. M. Livingstone, E. Hoehn, and R. Kipfer, 2011: Regime shift in groundwater temperature triggered by the

Arctic Oscillation. *Geophys. Res. Lett.,* **38,** L23401, doi:10.1029/2011GL049749.

Goddard, L., and N. E. Graham, 1999: Importance of the Indian Ocean for simulating rainfall anomalies over eastern and southern Africa. *J. Geophys. Res.,* **104** (D16), 19 099–19 116.

Hastenrath, S., 2007: Circulation mechanisms of climate anomalies in East Africa and the equatorial Indian Ocean. *Dyn. Atmos. Oceans,* **43,** 25–35.

Hong, C. C., T. Li, LinHo, and J. S. Kug, 2008: Asymmetry of the Indian Ocean dipole. Part I: Observational analysis. *J. Climate,* **21,** 4834–4848.

Ibanez, F., J. M. Fromentin, and J. Castel, 1993: Application of the cumulated function to the processing of chronological data in oceanography. *C. R. Acad. Sci., Ser. III,* **316,** 745–748.

Janowiak, J. E., 1988: An investigation of interannual rainfall variability in Africa. *J. Climate,* **1,** 240–255.

Jolliffe, I. T., 1986: *Principal Component Analysis.* Springer-Verlag, 271 pp.

Kalnay, E., and Coauthors, 1996: The NCEP/NCAR 40-Year Reanalysis Project. *Bull. Amer. Meteor. Soc.,* **77,** 437–471.

Kijazi, A. L., and C. J. C. Reason, 2009: Analysis of the 1998 to 2005 drought over the northeastern highlands of Tanzania. *Climate Res.,* **38,** 209–223.

Latif, M., D. Dommenget, M. Dima, and A. Grotzner, 1999: The role of Indian Ocean sea surface temperature in forcing East African rainfall anomalies during December–January 1997/98. *J. Climate,* **12,** 3497–3504.

Manatsa, D., W. Chingombe, H. Matsikwa, and C. H. Matarira, 2007: The superior influence of Darwin sea level pressure anomalies over ENSO as a simple drought predictor for southern Africa. *Theor. Appl. Climatol.,* **92,** 1–14, doi:10.1007/s00704-007-0315-3.

——, B. Chipindu, and S. K. Behera, 2012: Shifts in IOD and their impacts on association with East Africa rainfall. *Theor. Appl. Climatol.,* **110,** 115–128, doi:10.1007/s00704-012-0610-5.

Mapande, A. T., and C. J. C. Reason, 2005: Interannual rainfall variability over western Tanzania. *Int. J. Climatol.,* **25,** 1355–1368.

McKee, T. B., N. J. Doesken, and J. Kleist, 1993: The relationship of drought frequency and duration to time scales. Preprints, *Eighth Conf. on Applied Climatology,* Anaheim, CA, Amer. Meteor. Soc., 179–184.

Mutai, C. C., and M. N. Ward, 2000: East African rainfall and the tropical circulation/convection on intraseasonal to interannual timescales. *J. Climate,* **13,** 3915–3939.

——, ——, and A. W. Colman, 1998: Towards the prediction of the East African short rains based on sea-surface temperature–atmosphere coupling. *Int. J. Climatol.,* **18,** 975–997.

Nakamura, N., H. Kayanne, H. Iijima, T. R. McClanahan, S. K. Behera, and T. Yamagata, 2009: Mode shift in the Indian Ocean climate under global warming stress. *Geophys. Res. Lett.,* **36,** L23708, doi:10.1029/2009GL040590.

——, ——, ——, ——, ——, and ——, 2011: Footprints of IOD and ENSO in the Kenyan coral record. *Geophys. Res. Lett.,* **38,** L24708, doi:10.1029/2011GL049877.

Overland, J., S. Rodionov, S. Minobe, and N. Bond, 2008: North Pacific regime shifts: Definitions, issues and recent transitions. *Prog. Oceanogr.,* **77,** 92–102.

Reason, C. J. C., R. J. Allan, J. A. Lindesay, and T. J. Ansell, 2000: ENSO and climatic signals across the Indian Ocean basin in the global context: Part 1. Inter-annual composite patterns. *Int. J. Climatol.,* **20,** 1285–1327.

Rodionov, S. N., 2004: A sequential algorithm for testing climate regime shifts. *Geophys. Res. Lett.,* **31,** L09204, doi:10.1029/2004GL019448.

Shongwe, M. E., G. J. van Oldenborgh, B. van den Hurk, and M. van Aalst, 2011: Projected changes in mean and extreme precipitation in Africa under global warming, Part II: East Africa. *J. Climate,* **24,** 3718–3731.

Vicente-Serrano, S. M., J. C. González-Hidalgo, M. de Luis, and J. Raventós, 2004: Drought patterns in the Mediterranean area: The Alencia region (eastern Spain). *Climate Res.,* **26,** 5–15.

Vuille, M., M. Werner, R. S. Bradley, R. Y. Chan, and F. Keimig, 2005: Stable isotopes in East African precipitation record Indian Ocean zonal mode. *Geophys. Res. Lett.,* **32,** L21705, doi:10.1029/2005GL023876.

Webster, P. J., A. M. Moore, J. P. Loschnigg, and R. R. Leben, 1999: Coupled ocean–atmosphere dynamics in the Indian Ocean during 1997–98. *Nature,* **401,** 356–360.